Rising mm-Wave Era for Sensing/Networking with Multi-Facet System/Technology Challenges

Mau-Chung Frank Chang

Department of Electrical and Computer Engineering, University of California, Los Angeles, Los Angeles, CA 90095
Email: mfchang@ee.ucla.edu; Phone: (310) 794-1633

Keywords: mm-Wave System-on-Chip (SoC); Radio and Radar; Spectrometer; Interconnect; Plastic Waveguide

Abstract

The ever-increasing bandwidth requirement due to explosively growing 5/6G and AIoT data flows has compelled global commission authorities to release EM-spectra up to millimeter-wave (30-300GHz) and even (sub)-millimeter-wave frequency regimes (>300GHz) for massively expanded sensing and network applications. In this talk, we will exemplify System-on-Chip (SoC) developments at UCLA for multi-broadband radio, radar, interconnect, imaging and spectrometry at (sub)-mm-Wave frequencies based on state-of-the-art CMOS IC and packaging technologies. We will also address challenges encountered in both design and implementation that may hinder further development of such systems, especially the major shortcoming in super-scaled CMOS with limited dynamic range and power handling capability. We propose to replace silicon CMOS drain with selectively grown wide bandgap GaN for improved breakdown voltages and elucidating the "*Best Junction for the Function*" within the active device to acquire the desired sensing/network system performance/cost-effectiveness.

INTRODUCTION

In order to meet future 5/6G and AIoT sensing/networking needs, worldwide commission authorities have released multiple mm-Wave spectra, such as 5G's NR (New Radio) in FR2 and 6G's satellite/ground communication/control links via Ku, Ka, and V bands. These spectra possess distinctive properties from that of their microwave counterparts, including high propagation loss in air, high scattering/low penetration to metal/concrete objects, and high sensitivity to water/oxygen-rich environments.

In the past, III-V compound semiconductor MMICs were exclusively utilized for (sub)-mm-Wave circuit and systems. Nevertheless, the continuous scaling has elevated super-scaled CMOS technology's cutoff frequencies into similar spectrum ranges. As examples, we will share our recent developments in (sub)-mm-Wave radar, radio, imager, and wireless-interconnect based on state-of-the-art CMOS and packaging technologies. We will also address challenges encountered in both design and implementations that may hinder further development of aforementioned systems.

Our (sub)-mm-Wave SoCs were developed primarily through the partnership with NASA/JPL to satisfy the stringent spaceborne system requirements in size, weight, and power (SWaP)[1]. The infusion of silicon SoC has transformed space instrument design by monolithically integrating micro/mm-Wave, mixed-signal, and memory circuits to operate under low supply voltages (e.g. 1V), which is ideal for payload limited space probes. For instance, in Fig. 1, a 183-GHz spectrometer made of a heterodyne radiometer and a processor has been integrated in 28nm CMOS for planetary science investigation.

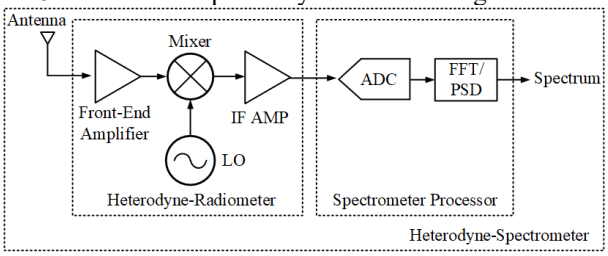

Fig. 1. General block diagram of heterodyne-radiometer/spectrometer.

Another application is to detect snow/water distributions for environmental science based on drones or unmanned vehicles (UAV). A Ku-band FMCW radar is realized to measure the depth/density of snow to estimate the amount of water available from mountain snow.

In the past, high-speed and short distance connectivity were fulfilled by mechanical connectors and cables with constraints in weight/size/rigidity and re-configurability. Such constraints can now be removed with mm-Wave contactless SoC radios. After a decade of our research effort, contactless connectors are finally commercialized in LG's 5G smartphones to enable dual-screens and Acer's laptops to allow 360° rotatable monitors.

HETERODYNE-RADIOMETER/SPECTROMETER

Radiometric observation at mm-wave is invaluable for assessing water vapor distribution inside storm/hurricanes. Mm-Wave radiometers can also sense water content on comets or planets. Unlike the conventional direct-detecting radiometer, heterodyne-radiometers made of mixers and LOs can pair with spectrometer processors to resolve the rotational emission/absorption spectra of ionized species and gas molecules [2]. The spectrometer processor (Fig.1) contains ADC, FFT/PSD processor, and accumulator.

W-BAND CMOS RADIOMETER AND PASSIVE IMAGER

A W-band CMOS radiometer is paired with a 35-nm InP HEMT LNA to achieve required noise performance [3]. The block diagram of such a W-band heterodyne-radiometer is shown in Fig. 1. A PLL is used to generate LO from 90 to 100GHz. The entire CMOS radiometer was packaged in a waveguide (Fig. 2). Coupling between WR10 waveguide and SoC input is accomplished with a probe via a microstrip line fabricated on alumina substrate. In order to characterize radiometer's noise temperature, a WR10 noise source (Quistar QNS10) is employed with and without the InP LNA. Results of both measurements are plotted in Fig. 3(a). In Fig. 3(b), the captured image demonstrates an integration/ performance-effective passive imager for the first time. The integrated system is configured with an angular (Az/El) raster scanner and a standard 25-dBi WR10 horn antenna.

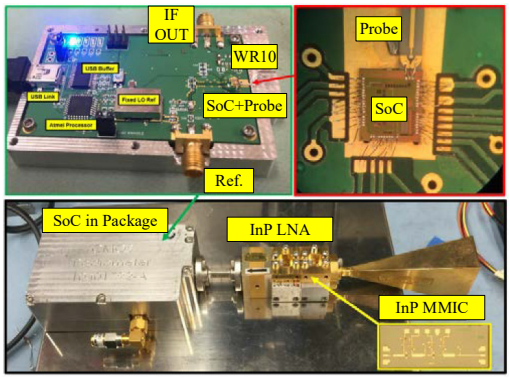

Fig. 2. Packaging details of a passive imager SoC and coupling to the InP LNAs.

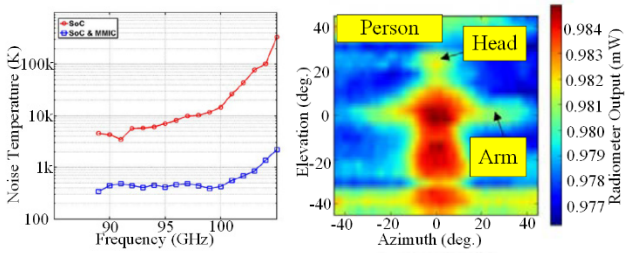

Fig. 3. (a) Measured noise temperature, and (b) captured passive image.

6-GS/S 4096-POINT SPECTROMETER PROCESSOR

The block diagram of our CMOS spectrometer processor is shown in Fig. 4, with an interleaved-by-2 flash ADC to convert incoming differential signals to seven-level thermometer-codes with 3 bit resolution at 6-GS/sec [4]. The full-speed thermo-coded digital signals are de-multiplexed by two initially (overall 4-ways because of 2-channel ADC being implemented), decoded into 3-bit binary form, and further de-multiplexed by 8-ways. Consequently, the FFT/PSD processor receives 32 parallel data streams, each at 187.5-MHz clock speed. For the FFT/PSD processor, the Cooley-Tukey algorithm is implemented with symmetric frequency bins removed. The spectrometer was prototyped in 65-nm CMOS and assembled as a module as shown in Fig. 5(a) and (b), respectively.

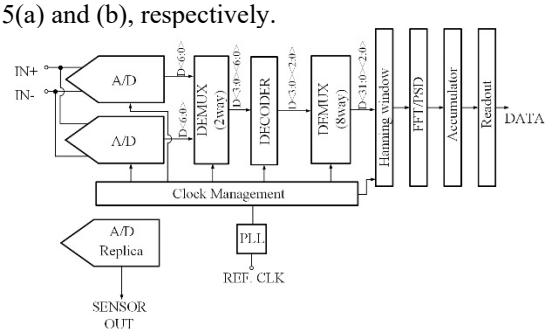

Fig. 4. Block diagram of a spectrometer processor

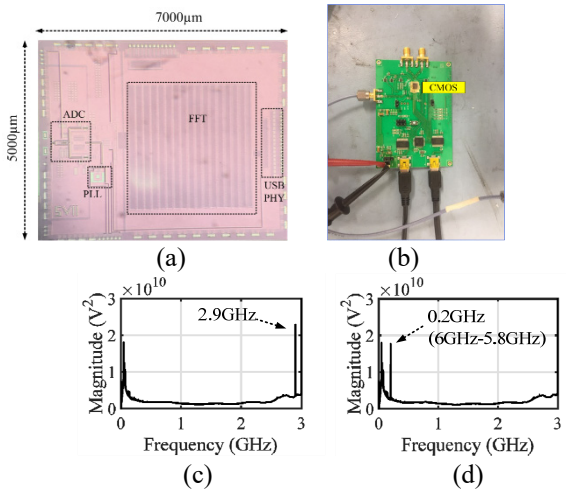

Fig. 5. (a) Fabricated spectrometer in 65-nm CMOS; (b) assembled spectrometer processor; (c) 2.9-GHz input tone measurement; (d) 5.8-GHz input tone measurement for frequency folding.

183-GHZ CMOS/INP-HYBRID HETERODYNE-SPECTROMETER

Connecting with the 6-GS/s spectrometer, a 183-GHz heterodyne-spectrometer is realized to measure rotational spectroscopic responses of water vapor and other important volatiles including organics, transient radical species. The fabricated CMOS receiver is shown in Fig. 6(a), and the complete heterodyne-spectrometer assembly is shown in Fig. 6(b). The measured noise temperature is shown in Fig. 6(c). The entire system's noise temperature ranges from 700 to 1000K within 1-GHz IF bandwidth. The 183GHz heterodyne-radiometer consumes 515mW, and the entire heterodyne-spectrometer consumes 3.315W. The complete system is eventually installed in a gas cell for the molecule detection. The observed response for the water vapor line at 183.31-GHz is depicted in Fig. 6(d).

With the measured system noise temperature (~1000K), the stratospheric water signal's (~100K) brightness should be readily observable with a sub-second integration time.

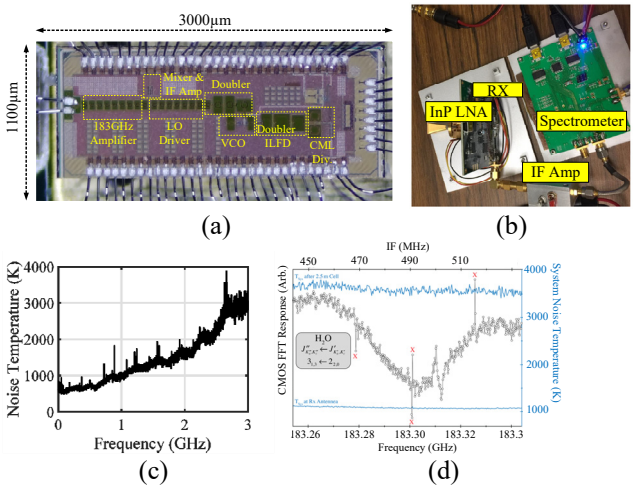

Fig. 6. (a) Fabricated 183-GHz heterodyne-radiometer; (b) assembled complete heterodyne-spectrometer; (c) measured noise temperature; and (d) detected water molecule.

Snow Sensing Radar

While the climate change has influenced a large portion of Earth in terms of temperature and sea water level, some of the most dramatic effects have appeared in the snowpack reduction and subsequent water availability globally. As snowpack retreats, the available water from snowmelt is limited, so more vigorous water resource management is required to ensure that water demands are satisfied. The key to this planning exercise is to accurately estimate the water content snowpack. Among the three major snow properties (cover, depth, density), a Ku-band FMCW radar is designed to measure the depth of snow [7]. As the frequency of radar operation increases beyond the Ku-band regime, an inter-grain scattering mechanism starts to dominate over the bulk absorption (Mie regime) for typical snow grain size, which is the reason to select the Ku-band for penetration.

The radar system targets a 7.5cm axial resolution, which results in a chirp bandwidth of 2GHz. To achieve a compact transceiver while supporting such a wide chirp bandwidth, a ring oscillator based chirp generation is adopted. The synthesizer accepts a low frequency reference chirp from the DDFS, synthesizes, and interpolates to turn a discrete frequency staircase into a smooth frequency ramp at Ku-band. The overall system block diagram is shown in Fig. 7. The fabricated radar transceiver in 65-nm CMOS, shown in Fig. 8(a), integrates DDFS, DAC, synthesizer, mixer, and amplifiers. The entire CMOS radar consumes 250-mW under 1.1-V supply. The assembled module is shown in Fig. 8(b). The ring oscillator's phase noise becomes problematic when there are secondary scatters around targets of interests. Such noise was largely overcome by the range correlation effect as shown in Fig. 8(c). The developed radar has adequately detected the depth of snow in Mammoth Mountain, as shown in Fig. 8(d).

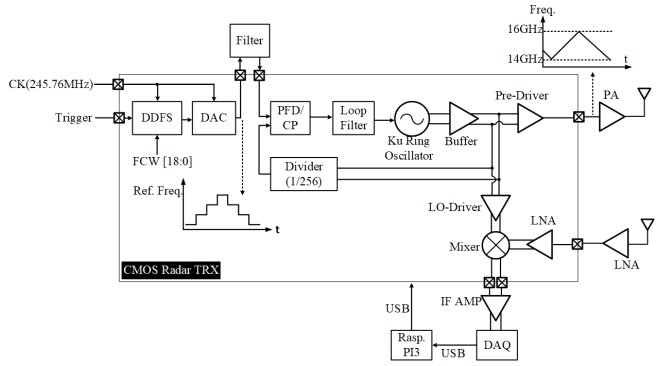

Fig. 7. Block diagram of Ku-band FMCW snow radar.

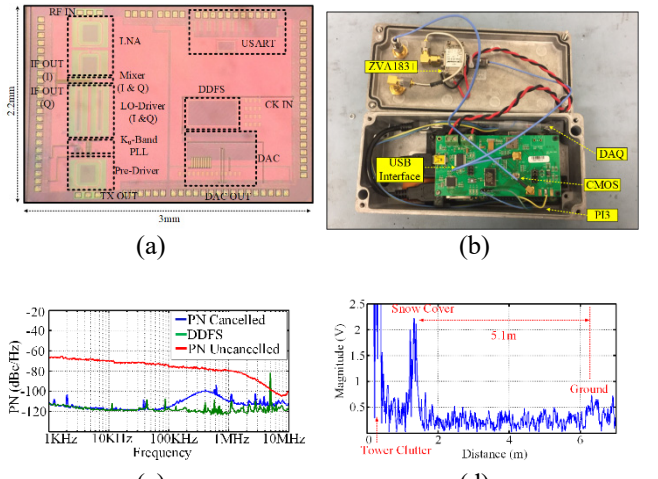

Fig. 8. (a) Fabricated CMOS FMCW radar; (b) assembled radar module; (c) measured phase noise cancellation; and (d) measured depth of snow.

Contactless/Waveguide Communications

Contactless connectivity is considered as the last-millimeter communication. Although successfully deployed to the public, the existing solution is lacking in terms of throughput (currently support 6-Gb/s) for the latest standard (e.g. 10-GB/s for USB-3.0) and thus requires a new direction to scale the communication bandwidth. Higher-depth modulations are attractive, but as illustrated in Fig. 9(a), multi-level signals typically suffer system non-linearity and amplitude distortion. To circumvent such limitations, a digital pre-distortion (DPD) algorithm is integrated into the PAM-4 modulator [8]. As shown in Fig. 9(b), the transmitter is built upon the RF-mixing-DAC, where the current-steering DAC is combined into the up-conversion mixer [9]. The PAM-4 modulator consists of a binary to 3-bit thermometer-code converter, three current sources, and three switches. The thermometer-coded data decides which current branch to flow and create four-level current signals at the mixer's input. The 8-bit R-2R DACs control the amount of each current and enable DPD.

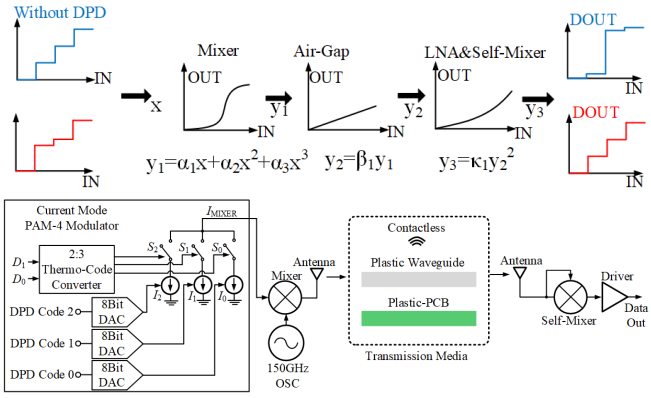

Fig. 9. (a) System concept with and without DPD; and (b) block diagram of 150-GHz CMOS PAM-4 TX/RX with current-mode DPD.

The 150-GHz transmitter and receiver are fabricated in 28-nm CMOS process, as shown in Fig. 10(a). The CMOS chips and antennas are assembled on the same PCB substrate, as shown in Fig. 10(b). In Fig. 10(c), without DPD, the upper-eye is completely closed and center-eye is wide open. After DPD applied, a 30-Gb/s communication over 1-mm air-gap is achieved with 2-pJ/bit energy efficiency. The communication distance can be extended by simply inserting plastic waveguides between the module, and the measured eye-diagram is captured in Fig. 10(e).

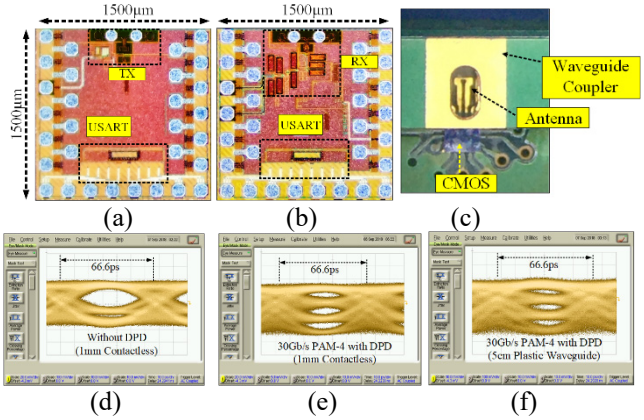

Fig. 10. (a) Fabricated chips; (b) assembled module; (c) measured without DPD; (d) measured with DPD; and (e) measured via plastic waveguide.

CONCLUSION

CMOS technologies will continue to pave ways in building high performance/cost-effective SoC for (sub)-mm-Wave sensing and communication systems. However, there are clear shortcomings in super-scaled CMOS with very limited dynamic range and power handling capability for signal transmissions. To alleviate such critical constraints, we propose to replace silicon CMOS drain with selectively grown wide bandgap GaN for much improved breakdown voltages (i.e. dynamic operation ranges) as shown in Fig. 11. With a proper lateral LDD type drain structure and doping designs, the simulated drain breakdown voltage can be elevated exceeding 30 volts (TABLE I), which is sufficient for implementing various power transmitters required by future multi-giga-hertz broadband 5/6G and AIoT mobile systems.

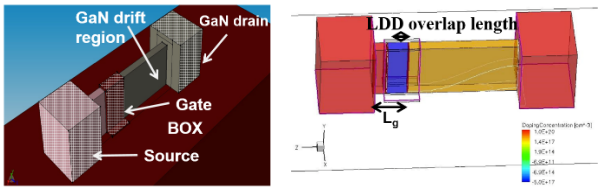

Fig. 11. Schematics of Lg=32nm GaN LD Drain FinFET

TABLE I

Device Parameters	Values
Physical gate length (L_g)	32nm
LDD length	100nm
Gate dielectric thickness (t_{OX})	2nm
Channel doping concentration	$5x10^{17}cm^{-3}$
S/D doping concentration	$1x10^{20}cm^{-3}$
LDD doping concentration	$1x10^{18}cm^{-3}$
V_{GS}/V_{DS}	0V/30V

REFERENCES

[1] P. H. Siegel, "*THz instruments for space*," IEEE Trans. Antennas Propag., vol. 55, no. 11, pp. 2957-2965, Nov. 2007.

[2] S. Padmanabhan, et al., "*Radiometer payload for the temporal experiment for storms and tropical systems technology demonstration mission*," IEEE Int. Geosci. Remote Sens. Symp., 2017.

[3] A. Tang, et al., "*A W-band 65nm CMOS/InP-hybrid radiometer & passive imager*," IEEE MTT-S Int. Microw. Symp., 2016.

[4] Y. Zhang, et al., "*Integrated wide-band CMOS spectrometer systems for spaceborne telescopic sensing*," IEEE Trans. Circuits Syst. I, 2019.

[5] Y. Kim, et al., "*A 183-GHz InP/CMOS-hybrid heterodyne-spectrometer for spaceborne atmospheric remote sensing*," IEEE Trans. THz Sci. Technolo., 2019.

[6] G. Chattopadhyay, et al., "*Compact terahertz instrumets for planetary missions*," Proc. 9th Eur. Conf. Antennas Propag., 2015.

[7] Y. Kim, et al., "*A Ku-band CMOS FMCW radar transceiver for snowpack remote sensing*," IEEE Trans. Microw. Theory Tech., 2018.

[8] Y. Kim, et al., "*A millimeter-wave CMOS transceiver with digitally pre-distorted PAM-4 mouldation for contactless communications*," IEEE J. Solid-State Circuits, 2019.

[9] Y. Kim, et al., "*30Gb/s 60.2mW 151GHz CMOS transmitter/receiver with digitally pre-distorted current mode PAM-4 modulator for plastic waveguide and contactless communications*," IEEE MTT-S Int. Microw. Symp., 2019.